JOURNAL OF GEOPHYSICAL RESEARCH, VOL. 93, NO. C3, PAGES 2237–2246, MARCH 15, 1988

Towed Thermistor Chain Observations of Fronts in the Subtropical North Pacific

ROGER M. SAMELSON[1] AND CLAYTON A. PAULSON

College of Oceanography, Oregon State University, Corvallis

A thermistor chain was towed 1400 km through the eastern North Pacific subtropical frontal zone in January 1980. The observations resolve surface layer temperature features with horizontal wavelengths of 0.2–200 km and vertical scales of 10–70 m. The dominant features, which have horizontal wavelengths of 10–100 km, amplitudes of 0.2°–1.0°C, and random orientation, likely arise from baroclinic instability. Associated with them is a plateau below 0.1 cpkm in the horizontal temperature gradient spectrum. Strong temperature fronts O(1°–2°C/3–10 km) are observed near 33°N, 31°N, and 27°N. Temperature variability is partially density compensated by salinity, with the fraction of compensation increasing northward. There is evidence of vertical mixing during high winds. Temperature at 15-m depth is roughly normally distributed around the climatological surface mean, with a standard deviation of approximately 0.5°C. The standard deviation would correspond to an adiabatic meridional displacement of 80–100 km in the mean gradient. Horizontal temperature gradient at 15-m depth has maximum values in excess of 0.25°C/100 m and kurtosis near 80. In the band 0.10–1 cpkm, the 15-m gradient spectrum is inversely proportional to wave number, consistent with predictions from geostrophic turbulence theory, while the spectrum at 70-m depth has additional variance that is consistent with Garrett-Munk internal wave displacements.

1. INTRODUCTION

The North Pacific subtropical frontal zone is a band of relatively large mean meridional upper ocean temperature and salinity gradient centered near 30°N [*Roden*, 1973]. Its existence is generally attributed to wind-driven surface convergence and large-scale variations in air-sea heat and water fluxes [*Roden*, 1975]. A recent attempt has been made to determine the associated large-scale geostrophic flow [*Niiler and Reynolds*, 1984], and hydrographic surveys [*Roden*, 1981] of the subtropical frontal zone have revealed energetic mesoscale eddy fields. However, little is known about the dynamics of the local mesoscale circulation or the detailed structure, generation, and dissipation of individual frontal features.

Here we report on an investigation of the upper ocean thermal structure of fronts in the North Pacific subtropical frontal zone. Observations were made in January 1980 with a towed thermistor chain that measured temperature at 12 to 21 depths in the upper 100 m of the water column. The thermistor chain was towed a distance of 1400 km in an area of the Pacific bounded by 26° and 34°N, 150° and 158°W. The observations resolve surface layer temperature features with horizontal wavelengths of 0.2–200 km and vertical scales of 10–70 m.

We use the term "frontal zone" rather than "front" because these wintertime measurements show randomly oriented multiple surface fronts up to 2°C in magnitude and less than 10 km in width. *Niiler and Reynolds* [1984] remark that as conductivity-temperature-depth (CTD) surveys of the frontal zone achieved "a consistently better resolution, a more complex synoptic detail was revealed." This holds true for the towed observations we report here. The horizontal wave number spectrum of surface temperature has three distinct bands. The energy-containing band, which is likely directly related to the baroclinic eddy field, extends to wavelengths as small as 10 km.

The towed thermistor chain and data collection procedure are described in section 2. Section 3 is devoted to a description of the fronts, their magnitude and horizontal scales, temperature-salinity compensation, vertical stratification, and response to wind. Probability densities of surface (15 m) temperature (with the climatological mean removed) and surface temperature gradient are presented in section 4.1. Horizontal wave number spectra of temperature and temperature gradient at several depths between 15 and 70 m are presented in section 4.2. In section 5 the high–wave number tail of the temperature spectrum is compared with the predictions of the theory of geostrophic turbulence [*Charney*, 1971].

2. INSTRUMENTATION AND DATA COLLECTION

The thermistor chain tows were made during Fronts 80, a multi-investigator endeavor focused on the subtropical frontal zone near 31°N, 155°W, in January 1980. Measurements by other investigators included CTD surveys [*Roden*, 1981], remotely sensed infrared radiation [*Van Woert*, 1982], expendable current profiler velocity profiles [*Kunze and Sanford*, 1984], and drifting buoy tracks [*Niiler and Reynolds*, 1984].

The thermistor chain has been described by *Paulson et al.* [1980]. The chain was 120 m long, with a 450-kg lead depressor to maintain a near-vertical alignment while it was towed behind the ship. Sensors were located at approximately 4-m intervals over the lower 82 m. These sensors included 27 Thermometrics (Edison, N. J.) P-85 thermistors and three pressure transducers. The thermistors have a response time of 0.1 s, relative accuracy of better than 10^{-3} °C, and absolute accuracy of roughly 10^{-2} °C. Data were recorded at a sampling frequency of 10 Hz. For this analysis, individual thermistor data records were averaged to values at 100-m intervals using ship speed from 2-hourly positions interpolated from satellite fixes. This speed varied from 2 to 6 m s^{-1}, so the number of data points in an averaged value varied from 166

[1] Now at Woods Hole Oceanographic Institution, Woods Hole, Massachusetts.

Paper number 7C0940.
0148-0227/88/007C-0940$05.00

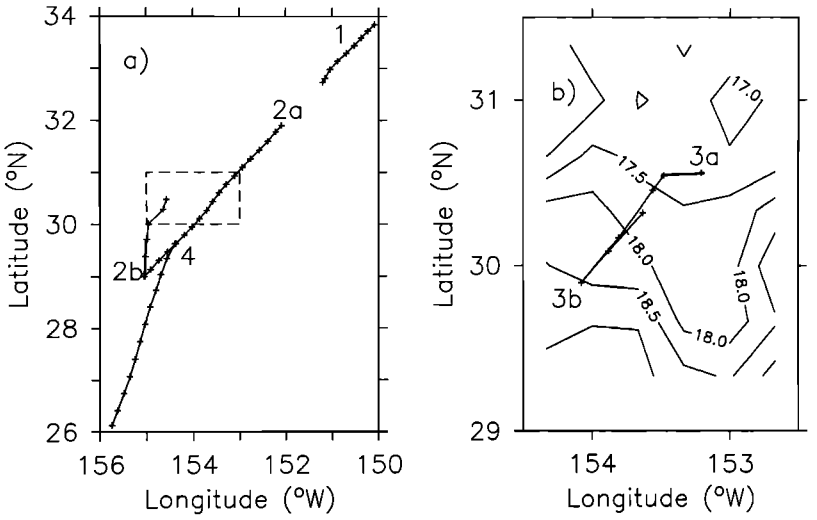

Fig. 1. Tow tracks. Crosses show 2-hourly positions. (Table 1 lists start and finish positions and times.) (*a*) Tows 1, 2a, 2b, and 4. The ship remained within the dashed rectangle during January 19–26. (*b*) Tows 3a and 3b. Isotherms at 20 m are from the CTD survey of *Roden* [1981].

to 502. The averaging removed the effects of ship roll and pitch and surface gravity waves. A maximum of 21 and a minimum of 12 thermistors functioned for entire tows. Thermistor depths were obtained from the ship's log speed and a model of the towed chain configuration calibrated by data from the pressure transducers. Temperature measurements were obtained at maximum and minimum depths of 95 m and 4 m.

The tow tracks are displayed in Figure 1. The four tows are labeled by number in chronological order. Since the tracks for tows 2 and 3 overlap, the track for tow 3, which took place on January 25, is displayed separately, overlaid on a contour of temperature at 20 m from the Roden CTD survey during January 24–30. Tows 2 and 3 are each divided into sections, labeled a and b, by course changes. The tow start and finish positions and times are given in Table 1. During January 19–26, the ship remained within the rectangle indicated by dashed lines in Figure 1.

Surface salinity was determined from temperature and conductivity measured by a Bisset Berman CTD located in the ship's wet lab, to which water was pumped from a sea chest at approximately 5-m depth. The cycle time for the fluid in this system was roughly 5–10 min during most of the experiment. The CTD temperature, corrected for (approximately 1°C) intake warming by comparison with data from the uppermost thermistor, was used to obtain surface density. CTD conductivity and temperature were recorded hourly (once every 10–20 km at typical tow speeds), as were surface wind speed and direction (from an anemometer at 34.4-m height), dry and wet bulb air temperatures, and incident solar radiation.

TABLE 1. Tow Start and Finish Positions and Times

Tow	Time, UT	North Latitude	West Longitude
1	0040 Jan. 16	33°51′	150°05′
	1600 Jan. 16	32°44′	151°12′
2a	0520 Jan. 17	31°54′	152°05′
2b	1655 Jan. 18	29°00′	155°03′
	0245 Jan. 19	30°28′	154°38′
3a	0700 Jan. 25	30°34′	153°12′
3b	1312 Jan. 25	29°53′	154°05′
	1700 Jan. 25	30°19′	153°38′
4	1900 Jan. 27	29°38′	154°24′
	1650 Jan. 28	26°07′	155°45′

3. Observations

3.1. *Surface Temperature, Salinity, and Density*

Sea surface temperature and salinity from shipboard CTD measurements during January 16–28 are displayed with contours of σ_t (density) in Figure 2. The data range over 7°C in temperature (T) and 1 part per thousand (ppt) in salinity (S). Though temperature may vary by 1°C at constant salinity, most of the data approximately obey a single identifiable T-S relation, with the exception of five points with $T > 20$°C, $S \simeq 35.1$ ppt, which are from a strong front at the southern end of tow 4. Salinity tends to compensate temperature, so density variations are relatively small, but warmer, more saline, water is typically less dense.

Surface temperature, salinity, and σ_t are displayed versus latitude in Figure 3. Scales have been chosen using the equa-

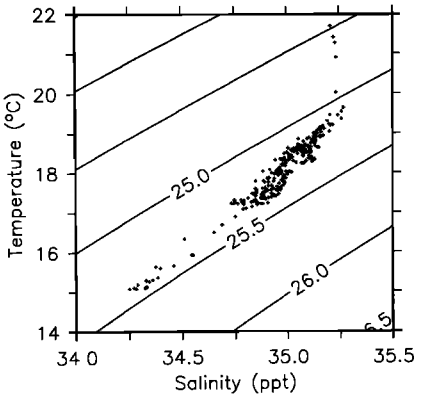

Fig. 2. Hourly sea surface temperature versus salinity from the onboard CTD during January 16–28, with contours of σ_t.

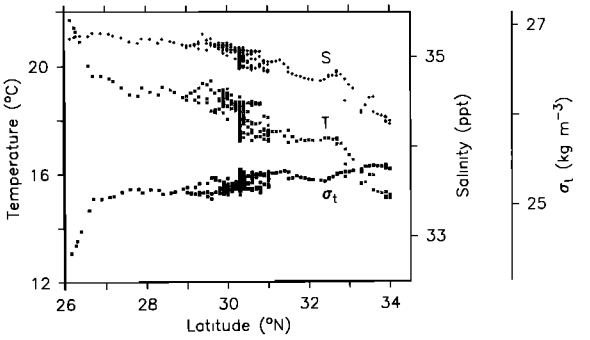

Fig. 3. Hourly sea surface temperature, salinity, and σ_t from the on-board CTD versus latitude.

tion of state so that a unit distance change in temperature (salinity) at constant salinity (temperature) corresponds approximately to a unit distance change in σ_t. Temperature and salinity tend to decrease toward higher latitudes, while density tends to increase. Features with smaller horizontal scales also show compensation. A partially compensated front near 30°N was crossed several times during January 19–27. (Its apparent sharpness is exaggerated by a set of measurements taken during frontal transects at constant latitude.) The temperature front near 33°N is roughly 70% compensated by salinity. In contrast, the 2°C front near 27°N has negligible salinity variation. There appears to be a density feature with roughly 300-km wavelength between 31°N and 34°N.

3.2. *Towed Thermistor Temperature at 15 and 70 m*

For each of the tows, Figure 4 displays 500-m horizontal averages of 15-m and 70-m thermistor temperature versus distance along the tow track. These are respectively the shallowest and deepest depths at which thermistor measurements were made during all four tows. The dominant temperature features have horizontal wavelengths of 10–100 km, amplitudes of 0.2°–1.0°C, and no apparent preferred orientation with respect to the large-scale meridional temperature gradient. Satellite imagery of the subtropical frontal zone in January and February 1980 [*Van Woert*, 1981, 1982] show a sea surface temperature field composed of highly distorted isotherms (rather than isolated patches of random temperature).

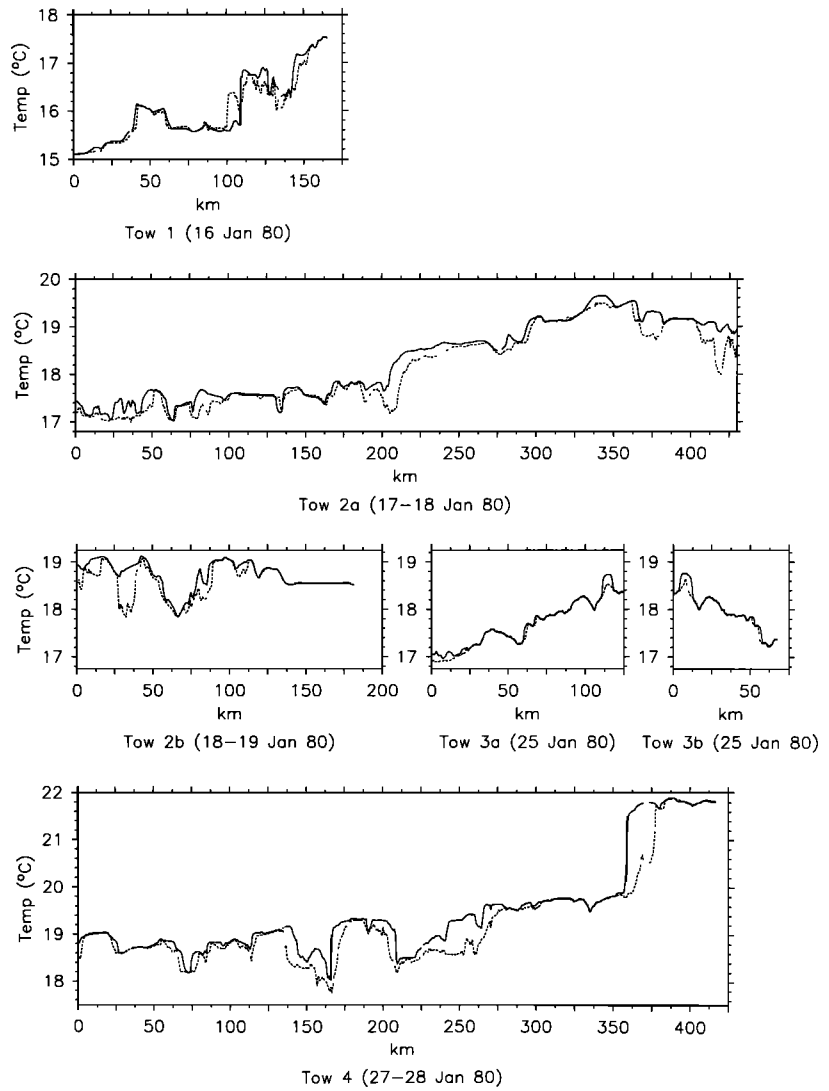

Fig. 4. Nominal 15-m (solid) and 70-m (dashed) thermistor temperature (horizontal 500-m means) versus distance along tow tracks. The large fronts in tow 1 near 125 km, tow 2a near 200 km, and tow 4 near 350 km are visible in Figure 3 near 33°N, 31°N, and 27°N, respectively.

The thermistor chain tows are cross sections of this field. In addition to the randomly oriented structures that dominate the field, there are several fronts with temperature changes of 1°C or more in the same sense as the large-scale gradient. These give a steplike appearance to the temperature record on horizontal scales of hundreds of kilometers.

The frontal meander that was crossed during tow 2b near 70 km is visible in an infrared satellite image from January 17, 1980 [*Van Woert*, 1982, Figure 2*a*]. The feature at 200 km in tow 2a is probably part of the same front, though it is obscured by cloud cover in the satellite image.

Tow 3 was made on January 25 through the frontal zone covered by a CTD survey [*Roden*, 1981] during January 24–31 (Figure 1*b*). The mean temperature gradient over tow 3 is roughly 10 times the large-scale meridional gradient. The sharp front at 18°C observed a week earlier at this location during tow 2a (near 200 km), does not appear in tow 3. Tows 3a and 3b, which were made roughly 6 hours apart in opposing directions on the same track, are very similar. This suggests that frontal features with horizontal scales as small as a few kilometers may have time scales longer than an inertial period.

3.3. *Stratification and Vertical Mixing*

The temperature difference between 15 m and 70 m was generally less than 0.1°C, except in regions near frontal features (Figure 4). During tow 1, larger differences appear only within 10–15 km of the surface fronts. During tow 2, some larger differences occur up to 25–30 km from fronts (though there may be closer fronts that lie off the tow track). In tow 4, as in tows 1 and 2, vertical temperature gradients are found consistently near surface fronts.

The absence of vertical gradients near fronts during the last 70 km of tow 2 and most of tow 3 is likely due to vertical mixing in response to high winds. For most of the experiment, wind speeds were 5–10 m s^{-1}. During the last period of tow 2b, they rose to 20 m s^{-1}, where they remained until after the tow was terminated. Wind speeds of 20 m s^{-1} were attained again 2 days prior to tow 3. Near fronts, a vertically mixed surface layer may restratify by gravitational adjustment of the horizontal density gradients, causing the vertical gradients observed in tows 1, 2, and 4.

Tows 2a and 3 overlap spatially with each other and with the Fronts 80 CTD surveys [*Roden*, 1981]. Between tows 2a (January 17–18) and 3 (January 25), local surface temperature decreased by approximately 1°C. *Roden* [1981] interprets a similar decrease of 0.5°C between the two CTD surveys (January 24–30 and January 31 to February 11) as southward advection of a tongue of cold water in a frontal meander. In both cases, 20 m s^{-1} wind speeds were attained between the sets of measurements, so cooling by entrainment may also have contributed. *Large et al.* [1986] present evidence for large entrainment events in the North Pacific during the fall season. These appear to be shear mixing events driven by the near-inertial response of the upper ocean to storms.

3.4. *Examples of Frontal Structure*

Fronts in the boundary layer exhibit a rich variety of structure. Figure 5 displays three examples of frontal isotherm cross sections.

Figure 5*a* shows the front encountered near 27° N (350 km in tow 4, Figure 4). The horizontal temperature gradient at this front reached 1.5°C/3 km, with a temperature change

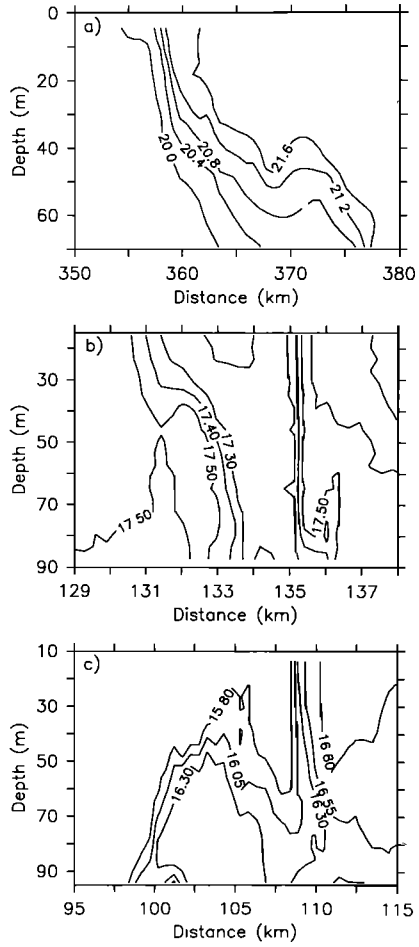

Fig. 5. Examples of fronts shown by isotherm cross sections (interpolated from horizontal 100-m mean thermistor temperatures) versus depth and distance along tow tracks. (*a*) Tow 4. This front is visible in Figure 3 near 27°N. (*b*) Tow 2a. (*c*) Tow 1.

of roughly 2°C over 10 km (Figure 4). The salinity change across this feature is small (Figure 3). The density change is approximately 0.5 kg m^{-3} over 10 km and dominates the variability in the surface density record (Figure 3). The geostrophic vertical shear across the front is roughly 10^{-2} s^{-1} at the surface.

Figure 5*b* displays the feature near 130 km in tow 2a. The temperature change across the front at 135 km is 0.25°C over 0.5 km. The temperature inversion at 132 km indicates an anomalous *T-S* relation. Note the difference in vertical structure of the two fronts at 132 and 135 km, which are only 3 km apart.

Figure 5*c* displays the feature near 110 km in tow 1. The surface front near 110 km is strongly salinity compensated. It is visible near 33°N in Figure 3. Measured horizontal temperature gradients at 15-m depth exceeded 0.25°C/100 m near 110 km and were the largest observed during the experiment. There is a 0.7°C temperature inversion, roughly 5 km wide, near 105 km. The presence of an inversion implies an anomalous local *T-S* relation, according to which the warmer, more saline water is denser. The warm, dense water most likely originated from the warm side of the front, with which it may be contiguous. The wind record suggests an Ekman flow to the southeast, nearly normal to the tow track, so that the

cooler surface water may have been advected over the warmer water from the northwest.

4. ANALYSIS

4.1. *Statistics*

To characterize the surface temperature variability statistically, we have calculated probability densities of temperature gradient and temperature deviation from climatology. Table 2 lists climatological surface temperatures for January and February from 100 years of ship observations and 27 years of hydrocasts [*Robinson*, 1976]. Figure 6 shows the probability density of the deviation of 15-m temperatures from a fit, linear in latitude in the intervals 25°–30°N and 30°–35°N, to the January climatology. As was noted by *Roden* [1981], the surface layer temperatures are colder on average than the climatological means. The apparent bimodality is probably due to poor statistics. The Kolmogorov-Smirnov goodness of fit test [*Hoel*, 1971] indicates that the distribution differs from normality at the 95% confidence level only if values less than 1.3 km apart are independent. The standard deviation is roughly 0.5°C.

Relative to the climatological gradient, a 0.5°C deviation would correspond to an adiabatic meridional displacement of 80–100 km. From drifters deployed near 30°N, 150°W, *Niiler and Reynolds* [1984] compute a mean northward surface velocity of 1–2 cm s^{-1} during January 27 through April 30, 1980. Examination of their Figure 9*a* suggests mean relative north-south drifter velocities of the same order over 100-km scales. From infrared imagery, *Van Woert* [1982] estimates an *e*-folding time of 60 days for a large frontal meander near 30°N during January and February 1980. The meridional displacement scale is comparable to the product of these velocity and time scales. Standard mixing-length arguments yield an eddy diffusivity (as velocity times length or length squared divided by time) of 1–2 × 10^3 m^2 s^{-1}. This is an order of magnitude smaller than typical values used in basin-scale numerical models [e.g., *Lativ*, 1987].

Horizontal 100-m mean temperature gradients were calculated from differences of adjacent 15-m temperatures. Figure 7 displays the probability density of these gradients. The dashed curve represents a Gaussian distribution with the observed mean and standard deviation. The observed kurtosis is 76, much larger than the Gaussian value of 3. This suggests the presence of a velocity field that strains the temperature gradients to small scales. The large kurtosis is characteristic of processes with sharp transitions between small and large values. It measures the frontlike nature of the surface temperature field, which is dominated by intermittent large gradients separated by regions of small gradients. Qualitatively similar distributions of temperature and velocity gradients occur at small scales in three-dimensional turbulence [*Monin and Yaglom*, 1975]. Calculations of the kurtosis for distributions of

TABLE 2. Climatological Sea Surface Temperature Averaged Over 150°–155°W [*Robinson*, 1976].

	North Latitude		
Month	25°	30°	35°
January	22.6	19.8	16.0
February	22.3	19.3	15.4

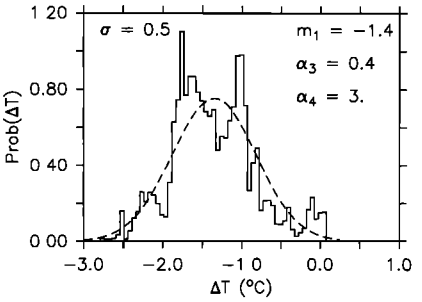

Fig. 6. Probability density of the difference of 15-m temperature from climatological surface temperature. The area under the solid curve is the fraction of occurrence. The dashed curve shows the Gaussian distribution with the same mean and standard deviation.

average horizontal gradient over distances from 100 m to 100 km show that the kurtosis increases smoothly toward smaller scales until a sharp change in dependence occurs at a few hundred meters. We interpret this scale as an average frontal width.

4.2. *Spectra*

Figure 8 displays the ensemble-averaged horizontal wave number spectrum of 15-m horizontal temperature gradient, band averaged to 5 bands per decade. The variability between 10- and 100-km wavelengths that is evident in the time series dominates the spectrum. At these wave numbers and at wave numbers above 1 cpkm, the spectrum is approximately constant. Between 0.1 cpkm and 1 cpkm, the spectrum is very nearly proportional to k^{-1}, where k is wave number.

We associate the low-wave number plateau with the mesoscale eddy field, the likely source of the dominant temperature features. The constant spectral level is a typical signature of an eddy production range, which may be driven by baroclinic instability. This instability generally prefers the scale of the internal deformation radius. The first local internal deformation radius, calculated using a Fronts 80 CTD station [*Roden*, 1980] for the upper 1500 m supplemented by deep data from a 1984 meridional transect [*Martin et al.*, 1987], is 40 km, which lies within the energetic plateau, toward its less resolved low-wave number end. There is other evidence for baroclinic instability in the eastern North Pacific. *Lee and Niiler* [1987] find unstable baroclinic waves with wavelengths of 60–200 km and *e*-folding times of 60–200 days in a linear analysis of perturbations of a 34-layer geostrophic model, and they include a review of recent observations and previous theoretical work.

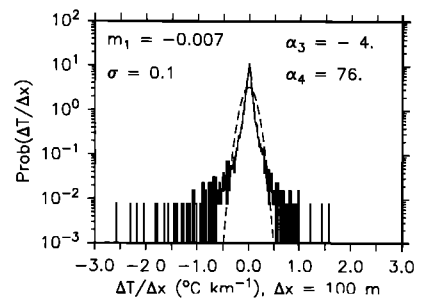

Fig. 7. Probability density of the 15-m horizontal temperature gradient. The area under the curve is the fraction of occurrence. The dashed curve shows the Gaussian distribution with the same mean and standard deviation.

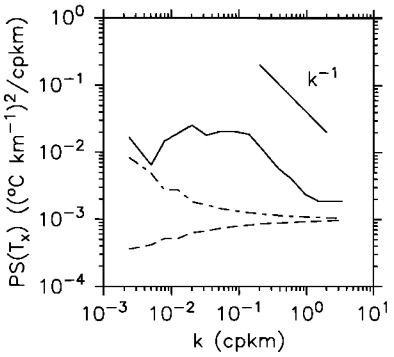

Fig. 8. Horizontal wavenumber spectrum of horizontal temperature gradient from tows 1, 2a, 2b, 3a, and 4, ensemble averaged and band averaged to 5 bands per decade. The slope of the -1 power law is indicated. Dashed lines show 95% confidence intervals.

The constant level at low wave numbers in the gradient spectrum corresponds to a k^{-2} slope in the temperature spectrum. Since the Fourier transform of a step function is roughly proportional to k^{-2}, this behavior could be interpreted as an artifact of the sharpness of the fronts rather than an indication of eddy generation. In that case, however, the k^{-2} behavior should persist to wave numbers comparable to the frontal widths (scales small enough that the fronts do not resemble step functions). Examination of the temperature record (Figure 4) suggests that frontal widths are no greater than a kilometer. The kurtosis calculations described in section 4.1 indicated widths of a few hundred meters. In contrast, the k^{-2} band is restricted to wave numbers of less than 0.1 cpkm, corresponding to scales an order of magnitude larger than the frontal widths. Thus this interpretation does not appear correct.

The break in slope at the high-wave number end of the plateau occurs near 0.1 cpkm, at roughly the fifth internal deformation radius. The constant spectral level at wave numbers above 1 cpkm is likely due to temperature gradient production in the surface boundary layer.

Figure 9 displays horizontal wave number spectra of 15-m horizontal temperature gradient from each individual tow, band averaged to 10 bands per decade. The spectral levels vary by roughly half a decade. The spectral shapes are nearly uniform, despite the apparent differences in the qualitative nature of the records noted in section 3 (e.g., the single large feature in tow 1 versus the myriad smaller features in tows 2a and 2b). Each spectrum has a broad peak or plateau at low wave number and a break in slope near 10 km, and each is approximately proportional to k^{-1} between 10 km and 1 km. A minimum occurs between 1-km and 350-m wavelengths in three of the five spectra. A secondary peak appears near 350 m in these three spectra, followed by a decrease toward the Nyquist wavelength (200 m). The spectra appear to fall off slightly toward wavelengths larger than 50 km. In this region, however, the number of data points is small and the 95% confidence intervals large. The spectrum from tow 3*b* is not shown. At the 95% confidence level it is indistinguishable from the tow 3a spectrum. Tows 3a and 3b were made on the same track a few hours apart (Figure 1*b*, Table 1) and are very similar (Figure 4). Hence we do not regard the two spectral estimates from tow 3 as independent and have included only the estimates from tow 3a in the ensemble average.

Figure 10 displays ensemble-averaged horizontal wave

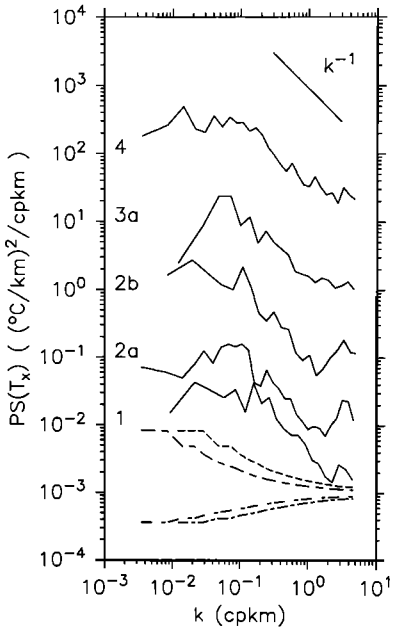

Fig. 9. Horizontal wavenumber spectra of horizontal temperature gradient from tows 1, 2a, 2b, 3a, and 4, band averaged to 10 bands per decade. Successive spectra are offset by 1 decade. The slope of the -1 power law is indicated. Dashed lines show 95% confidence intervals for the shortest (tow 3a) and longest (tow 2a) records.

number spectra of 15-m and 70-m temperature, band averaged to 5 bands per decade. We interpret the difference between the spectral levels at 15 m and 70 m in the bands above 0.1 cpkm as internal wave vertical displacements at 70 m. Since the average vertical temperature gradients are small at 15 m, less than 10^{-4} °C m^{-1} (at 70 m they are typically 10^{-2}–10^{-3} °C m^{-1}), and since the vertical internal wave velocities must vanish at the surface, temperature variance from internal wave isotherm displacement will be small at 15 m. If the 70-m spectrum is composed of the sum of an internal wave vertical displacement spectrum that is uncorrelated with the 15-m spectrum and a spectrum (due to other processes) equal in

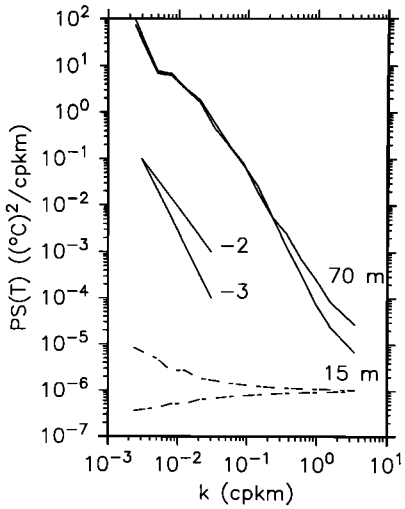

Fig. 10. Horizontal wave number spectra of 15-m and 70-m temperature for tows 1, 2a, 2b, 3a, and 4, ensemble averaged and band averaged to 5 bands per decade. Slope of -2 and -3 power laws are indicated. Dashed lines show 95% confidence intervals.

variance to the 15-m spectrum at each wave number, the 70-m internal wave spectrum will be the difference of the power spectra at 70 m and 15 m. (Differencing the series leads to an overestimate of the internal wave variance because incoherent parts not due to internal waves will contribute to the power spectrum of the differenced series.) Using average vertical temperature gradients at 70 m from entire tow means of surrounding thermistors to estimate displacements and the local buoyancy frequency, we obtain for tows 2 and 4 the internal wave energy spectral estimates shown in Figure 11. The empirical Garrett-Munk prediction [*Katz and Briscoe*, 1979, equation A12; *Garrett and Munk*, 1972], with *Desaubies'* [1976] parameters $r = 320$ m^2 h^{-1} and $t = 4 \times 10^{-4}$ cph cpm^{-1}, is plotted for comparison. The spectral levels are mostly within 2–3 times the predicted values, and the spectral slopes show excellent agreement. A large temperature inversion and small vertical gradients prevented reliable calculations for tows 1 and 3. Even in tows 2 and 4, average temperature differences of surrounding thermistors are not far from the noise level of the calibrations, so these estimates have limited value as measurements of internal wave energy. They are, however, consistent with the hypothesis that the difference in the 70-m and 15-m spectral levels in the 0.1- to 1-cpkm band is due to internal waves, and that the variance in the 15-m spectrum in this band is due to other processes. Below 0.1 cpkm, where the break in slope in the 15-m spectrum occurs, the internal wave energy appears to be negligible compared with thermal variance from other sources. This apparently fortuitous correspondence gives the 70-m spectrum a nearly uniform slope (Figure 10).

Figure 12 displays ensemble-averaged-spectra of horizontal temperature gradients at 15, 23, 31, 50, and 70 m, as well as ensemble-averaged coherence from cross spectra between the 15-m record and the others, all band averaged to 5 bands per decade. There is significant vertical coherence in the 0.1- to 1-cpkm band over most of the surface layer. Where the internal wave variance raises the spectral levels above the 15-m values, coherence decreases. This decrease occurs at successively shorter wavelengths for shallower thermistors, presumably since only short wavelength internal waves may exist on infrequent shallow patches of vertical gradient.

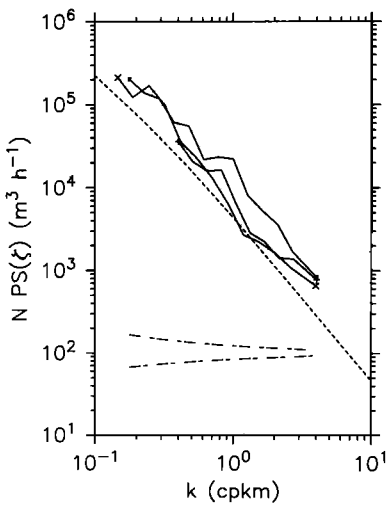

Fig. 11. Solid lines show estimated 70-m internal wave vertical displacement spectra from the difference of 70-m and 15-m power spectra, band averaged to 10 bands per decade (small crosses indicate tow 2a, plusses, tow 2b; large crosses, tow 4). Long-dashed lines show 95% confidence intervals; short-dashed lines show the Garrett-Munk canonical internal wave spectrum with $r = 320$ m^2 h^{-1}, $t = 4 \times 10^{-4}$ cph cpm^{-1}.

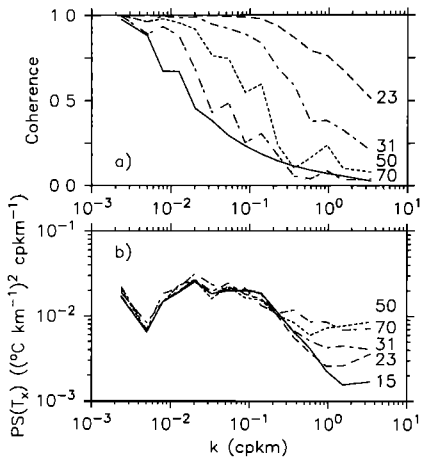

Fig. 12. Horizontal wave number spectra and coherence, ensemble averaged and band averaged to 5 bands per decade. (*a*) Dashed lines show coherence from cross spectra between 15-m and 23-, 31-, 50-, and 70-m horizontal temperature gradients. The solid line shows the 95% significance level for nonzero coherence. (*b*) Spectra of the horizontal temperature gradient at 15, 23, 31, 50, and 70 m. (95% confidence intervals as in Figure 8).

5. Three-Dimensional Geostrophic Turbulence

We have interpreted the low-wave number plateau in the 15-m horizontal temperature gradient spectrum (Figure 8) as the signature of the mesoscale eddy field and a probable baroclinic production range, and the high-wave number plateau as a surface boundary layer production range. At wave numbers above 0.1 cpkm, internal waves consistently account for the difference between the 70-m and 15-m spectra (Figures 10 and 11). It remains to explain the spectral slope in the 0.1- to 1-cpkm wave number band. In this band, the temperature gradient spectrum has 95% significant vertical coherence and is very nearly proportional to k^{-1} (Figures 8 and 9). *Charney* [1971] predicted a k^{-3} subrange in the potential energy spectrum for wave numbers above a baroclinic production range. If the potential energy spectrum has the same slope as the temperature spectrum in the 0.1- to 1-cpkm band, the observations will be consistent with this prediction, since the temperature spectrum (Figure 10) is proportional to k^{-2} times the temperature gradient spectrum.

Charney [1971] discovered a formal analogy that holds under certain conditions between the spectral energy evolution equations associated with the two-dimensional Navier-Stokes equations and the quasi-geostrophic potential vorticity ("pseudo-potential vorticity") equation. Using this analogy, he inferred the existence and spectral form of an inertial subrange in quasi-geostrophic motion from the results of *Kraichnan* [1967] on two-dimensional Navier Stokes turbulence. In the subrange, enstrophy (half-squared vorticity) is cascaded to small scales, rather than energy as in three-dimensional turbulence.

Charney introduced the phrase "geostrophic turbulence" to describe the energetic, low-frequency, high-wave number, three-dimensional, isotropic, quasi-geostrophic motions in the enstrophy cascade subrange. The phrase is now also used more generally to describe the "chaotic, nonlinear motion of

fluids that are near to a state of geostrophic and hydrostatic balance" [*Rhines*, 1979] but in which anisotropic waves (e.g., Rossby waves) may propagate. Large-scale geophysical fluid motions that are turbulent and strongly two-dimensional are also often described as "two-dimensional turbulence." Because they may contain Rossby wave motions, they need not satisfy Charney's criteria for the existence of an inertial subrange. Charney's theory applies strictly only to three-dimensional, quasi-geostrophic motion at scales small enough that the beta effect may be neglected.

In the predicted inertial subrange, the energy spectrum $E(k)$ has the form

$$E(k) = C\eta^{2/3}k^{-3} \tag{1}$$

where C is a universal constant, η is the enstrophy cascade rate, and k is an isotropic wave number. Total energy is equally distributed between the potential energy and each of the two components of kinetic energy. For a spatially oriented wave number (e.g., wave number along a tow track), the power law dependence is unchanged, but the traverse velocity kinetic energy component contains 3 times the energy of each of the longitudinal component and the potential energy component, so the total energy is 5 times the potential energy [*Charney*, 1971]. The potential energy may be expressed in terms of the density, using the hydrostatic balance and a local value of the buoyancy frequency N:

$$\text{(potential energy)} = (g/N)^2[(\rho - \rho_0)/\rho_0]^2 \tag{2}$$

where g is gravitational acceleration, ρ is density, and ρ_0 is a constant reference density.

The temperature and salinity data (Figure 2) indicate that relative temperature tends to determine relative density, at least on the 10- to 15-km scales of the salinity data. We have used linear regression T-S relations from these data to convert 15-m temperature to density. For tow 1 a single linear T-S relation was used; for tow 2, three relations; for tow 3, a single relation; and for tow 4, three relations. The change in spectral shape from this conversion was minimal. The spectral levels were altered, with tows 2 and 3 nearly equal and tows 1 and 4 roughly half and 3 times as large, respectively, as tows 2 and 3. (The large front near 26°N is intensified by the conversion to density and was excluded from the density spectra, as it imparts a strong k^{-2} signal to the spectrum and appears to belong to a dynamical regime different from that of the remainder of the observations.) The southward increase in surface density variance is consistent with *Niiler and Reynolds*' [1984] drifter observations of southward increasing eddy kinetic energy.

A relatively large uncertainty is associated with the choice of a value of N for the conversion (equation (2)) from density to potential energy. The Charney theory requires use of the local N, which is assumed to be slowly varying. In the mixed layer, N may be arbitrarily small, and at the mixed layer base, N is not slowly varying. We use $N = 2$ cph, which lies between the mixed layer and pycnocline values. Within the 95% confidence intervals, the resulting ensemble-averaged potential energy spectrum may be obtained directly by multiplying the 15-m temperature spectrum in Figure 10 by 10^3 cm s^{-2} °C^{-2}. The variance in the 0.1- to 1-cpkm band is roughly 3 cm^2 s^{-2}, and the corresponding predicted kinetic energy is 12 cm^2 s^{-2}. A velocity scale U formed from the square root of twice the kinetic energy is 5 cm s^{-1}, which yields a Rossby number ($Uk/f = 0.05$ at $k = 0.1$ cpkm) that is appropriate for quasi-geostrophic theory. For comparison, the square root of twice the *Niiler and Reynolds* [1984] drifter kinetic energy north of 30°N is 18 cm s^{-1}. This number is larger than 5 cm s^{-1}, as one might expect because it includes geostrophic motion at scales greater than 10 km, Ekman transport, and inertial oscillations. Assuming the universal constant C in (1) is equal to 1, we estimate the potential enstrophy transfer (dissipation) rate η as 2×10^{-16} s^{-3}. This lies between atmospheric estimates of 10^{-15} s^{-3} [*Charney*, 1971; *Leith*, 1971] and numerical ocean model values of 5×10^{-19} s^{-3} [*McWilliams and Chow*, 1981].

A temperature gradient variance dissipation rate may be estimated from the enstrophy dissipation rate, using the inverse of the temperature variance to kinetic energy conversion (2.5×10^{-4} s^2 °C^2 cm^{-2}) to estimate temperature gradient from vorticity, as 4×10^{-5} °C^2 km^{-2} d^{-1}. The temperature gradient variance in the wave number band 10^{-3}–10^{-1} cpkm is of the order of 2×10^{-3} °C^2 km^{-2} (Figure 8). If it is assumed (for simplicity and without detailed consideration of the dynamics) that all this temperature gradient variance cascades to small scales, the resulting decay time scale is 50 days. This is remarkably similar to the 60-day e-folding time scale estimated from satellite measurements for the evolution of a 100-km-wavelength frontal meander [*Van Woert*, 1982]. The dynamical relation between these two time scales is unclear.

The interpretation of the k^{-3} band (0.1–1.0 cpkm) in the temperature spectrum as a geostrophically turbulent inertial subrange appears to be consistent, with sensible values for velocity and dissipation rate resulting from the conversion from the temperature spectrum to an energy spectrum. It is supported by the identification of the k^{-2} band (10^{-3}–10^{-1} cpkm) as a baroclinic production range, since one expects a dynamical link between neighboring spectral bands. However, the interpretation should be viewed with caution. The density measurements do not extend to horizontal scales of less than 10 km. The predictive theory requires a slowly varying N and a flow isolated from boundary effects; these conditions may not apply here, though it is not evident that they are essential to the dynamics. There are alternative mechanisms that could generate temperature variance in the 0.1- to 1.0-cpkm band. These include near-inertial currents, variations in air-sea fluxes and entrainment, and advection by eddies that are dynamically independent of the surface temperature field (i.e., by which surface temperature is advected as a passive scalar).

Lagrangian motion due to near-inertial surface currents is not well understood. Absolute displacement of the surface temperature field by near-inertial currents with horizontal scales greater than 10 km will not affect the temperature spectrum in the band. Relative meridional displacements of 5–10 km in the mean temperature field, driven by near-inertial currents that have horizontal scales of 10 km and less, would be required to explain the variance. Over 900-km space and 2-week time scales and despite variable atmospheric conditions, the observed spectral shapes varied little, while near-inertial currents typically respond strongly to storms. Consequently, near-inertial currents appear to be an unlikely source of the variance.

At horizontal scales below 10 km, variations in air-sea fluxes should not be sufficient to create 0.05°C features in a mixed layer of 75- to 125-m depth. Over a day, this would require a differential heat flux of 200 W m^{-2}. Over days to weeks, atmospheric conditions are probably not coherent with oceanic surface temperature on 10-km horizontal scales. Variations in entrainment, such as those observed by *Large et al.* [1986], may produce mixed layer temperature variations, but

presumably mostly on scales larger than 10 km. Variations in mixed layer depth may produce temperature variations in response to a spatially constant heat flux. For a constant heat flux of 100 W m^{-2}, a 25% variation in mixed layer depth would result in a differential heating of 25 W m^{-2}, which would have to be maintained for more than a week to explain the observed variance. Hence variations in air-sea fluxes, entrainment, and mixed layer depth also appear to be unlikely sources of the variance.

For the geostrophic turbulence interpretation, temperature was assumed to be a dynamical variable, directly related to the density. Alternatively, it may be assumed to be a passive scalar, advected by a dynamically independent turbulent eddy field. If the dominant scales of the eddy field are larger than 10 km, dimensional analysis predicts a k^{-1} subrange in temperature at scales smaller than 10 km. The balance is between velocity shear at large scales and temperature dissipation at small scales. This is analogous to the viscous-convective subrange in isotropic turbulence [*Batchelor*, 1959]. However, the observed temperature spectrum has a k^{-3} slope, which does not agree with the dimensional analysis prediction for a passively advected scalar.

A k^{-3} dependence of surface temperature variance on wave number has been found by *Scarpace and Green* [1979] and *Holladay and O'Brien* [1975], both in upwelling regimes. Scarpace and Green found k^{-3} dependence for wave numbers of 1–25 cpkm in Lake Superior, where a typical internal deformation radius is only 5 km. Holladay and O'Brien found k^{-3} dependence for wave numbers of 0.05–0.25 cpkm off the central coast of Oregon.

6. SUMMARY

The thermistor tows yield a detailed two-dimensional description of surface layer temperature along 1400 km of tow tracks in the eastern North Pacific subtropical frontal zone during January 1980. In brief, we find:

1. The dominant features have wavelengths of 10–100 km, amplitudes of 0.2°–1.0°C, and no preferred orientation with respect to the mean meridional gradient (Figure 4). These features, which could be created from the climatological mean sea surface temperature field by adiabatic meridional displacements of roughly 100 km, likely arise from baroclinic instability of the geostrophic upper ocean flow. They form a plateau in the temperature gradient spectrum at wavelengths of greater than 10 km (Figure 8).

2. Strong temperature fronts are observed near 33°N, 31°N, and 27°N, with density compensation by salinity increasing northward (Figures 3 and 4). Maximum horizontal near-surface gradients exceed 0.25°C 100 m^{-1} (Figure 7). Near fronts, there is evidence of enhanced vertical mixing during periods of strong winds.

3. Temperature is roughly normally distributed around the climatological mean (Figure 6). The standard deviation of this distribution (0.5°C) would correspond to an adiabatic meridional displacement of 80–100 km in the mean gradient. The near-surface horizontal temperature gradient has kurtosis of near 80 (Figure 7).

4. In the band 0.1–1 cpkm, the near-surface temperature spectrum has the −3 power law form (Figures 8 and 10) predicted by *Charney* [1971] for energetic high-wave number near-geostrophic motion above a baroclinic production range. Horizontal temperature gradients have significant vertical coherence over the upper 50 m at all wavelengths and over the upper 70 m at wavelengths of greater than 5 km (Figure 12).

5. The departure at 70-m depth of the temperature spectrum from the −3 power law can be ascribed to internal wave vertical displacements that are consistent with the Garrett-Munk model of the internal wave spectrum (Figure 11).

Acknowledgments. This research was supported by the Office of Naval Research under contracts N00014-87-K-0009 and N00014-84-C-0218. Rick Baumann's assistance with data collection and analysis is gratefully acknowledged. The authors thank Gunnar Roden and Roland DeSzoeke for providing CTD data and Eric Kunze and Andrew Bennett for comments on the manuscript.

REFERENCES

Batchelor, G. K., Small-scale variation of convected quantities like temperature in a turbulent fluid, 1, *J. Fluid Mech.*, *5*, 113–139, 1959.

Charney, J. G., Geostrophic turbulence, *J. Atmos. Sci.*, *28*, 1087–1095, 1971.

Desaubies, Y. J. F., Analytical representation of internal wave spectra, *J. Phys. Oceanogr.*, *6*, 976–981, 1976.

Garrett, C., and W. Munk, Space-time scales of internal waves, *Geophys. Fluid Dyn.*, *2*, 225–264, 1972.

Hoel, P. G., *Introduction to Mathematical Statistics*, 4th ed., 409 pp., John Wiley, New York, 1971.

Holladay, C. G., and J. J. O'Brien, Mesoscale variability of sea surface temperatures, *J. Phys. Oceanogr.*, *5*, 761–772, 1975.

Katz, E. J., and M. G. Briscoe, Vertical coherence of the internal wave field from towed sensors, *J. Phys. Oceanogr.*, *9*, 518–530, 1979.

Kraichnan, R. H., Inertial ranges in two-dimensional turbulence, *Phys. Fluids*, *10*, 1417–1423, 1967.

Kunze, E., and T. B. Sanford, Observations of near-inertial waves in a front, *J Phys. Oceanogr.*, *14*, 566–581, 1984.

Large, W. G., J. C. McWilliams, and P. P. Niiler, Upper ocean thermal response to strong autumnal forcing of the northeast Pacific, *J. Phys. Oceanogr.*, *16*, 1524–1550, 1986.

Lativ, M., Tropical ocean circulation experiments, *J. Phys. Oceanogr.*, *17*, 246–263, 1987.

Lee, D. K., and P. P. Niiler, The local baroclinic instability of geostrophic spirals in the eastern North Pacific, *J. Phys. Oceanogr.*, *17*, 1366–1377, 1987.

Leith, C. E., Atmospheric predictability and two-dimensional turbulence, *J. Atmos. Sci.*, *28*, 145–161, 1971.

Martin, M., L. D. Talley, and R. A. de Szoeke, Physical, chemical and CTD data from the Marathon II expedition, *Data Rep. 131, Ref. 87-15*, Coll. of Oceanogr., Oreg. State Univ., Corvallis, 1987.

McWilliams, J. C., and J. H. S. Chow, Equilibrium geostrophic turbulence, I, A reference solution in a beta-plane channel, *J. Phys. Oceanogr.*, *11*, 921–949, 1981.

Monin, A. S., and A. M. Yaglom, *Statistical Fluid Mechanics*, vol. 2, 874 pp., MIT Press, Cambridge, Mass., 1975.

Niiler, P. P., and R. W. Reynolds, The three-dimensional circulation near the eastern North Pacific subtropical front, *J. Phys. Oceanogr.*, *14*, 217–230, 1984.

Paulson, C. A., R. J. Baumann, L. M. deWitt, T. J. Spoering, and J. D. Wagner, Towed thermistor chain observations in Fronts 80, *Data Rep. 85, Ref. 80-18*, 183 pp., Sch. of Oceanogr., Oreg. State Univ., Corvallis, 1980.

Rhines, P. B., Geostrophic turbulence, *Annu. Rev. Fluid. Mech.*, *11*, 401–441, 1979.

Robinson, M. K., *Atlas of North Pacific Ocean Monthly Mean Temperatures and Mean Salinities of the Surface Layer, Ref. Publ. 2*, 19 pp., 173 figures, Nav. Oceanogr. Office, Dep. of the Navy, Washington, D. C., 1976.

Roden, G. I., Thermohaline structure, fronts, and sea-air exchange of the trade wind region east of Hawaii, *J. Phys. Oceanogr.*, *4*, 168–182, 1973.

Roden, G. I., On North Pacific temperature, salinity, sound velocity and density fronts and their relation to the wind and energy flux fields, *J. Phys. Oceanogr.*, *5*, 557–571, 1975.

Roden, G. I., Fronts expedition CTD data report 15 January–16 February 1980, *Tech. Rep. 384*, Univ. of Wash., Seattle, 1980.

Roden, G. I., Mesoscale thermohaline, sound velocity and baroclinic

flow structure of the Pacific subtropical front during the winter of 1980, *J. Phys. Oceanogr.*, *11*, 658–675, 1981.

Scarpace, F. L., and T. Green III, The spatial variability of coastal surface water temperature during upwelling, *J. Phys. Oceanogr.*, *9*, 638–643, 1979.

Van Woert, M. L., Satellite observations in Fronts 80, *SIO Ref. 81-38*, 41 pp., Scripps Inst. of Oceanogr., La Jolla, Calif., 1981.

Van Woert, M., The subtropical front: Satellite observations during Fronts 80, *J. Geophys. Res.*, *87*(C12), 9523–9536, 1982.

C. A. Paulson, College of Oceanography, Oregon State University, Corvallis, OR 97331.

R. M. Samelson, Woods Hole Oceanographic Institution, Woods Hole, MA 02543.

(Received July 2, 1987;
accepted December 11, 1987.)